Supplementary Material for "Rabi oscillations in a superconducting nanowire circuit"

Yannick Schön,[1] Jan Nicolas Voss,[1] Micha Wildermuth,[1] Andre Schneider,[1] Sebastian T. Skacel,[1] Martin P. Weides,[1,2] Jared H. Cole,[3] Hannes Rotzinger,[1,4,*] and Alexey V. Ustinov[1,5,6]

[1] *Physikalisches Institut, Karlsruhe Institute of Technology, 76131 Karlsruhe, Germany*
[2] *School of Engineering, University of Glasgow, Glasgow, G12 8QQ, United Kingdom*
[3] *Chemical and Quantum Physics, School of Science, RMIT University, Melbourne, Victoria, 3001, Australia*
[4] *Institute for Quantum Materials and Technologies, Karlsruhe Institute of Technology, 76131 Karlsruhe, Germany*
[5] *National University of Science and Technology MISIS, Moscow 119049, Russia*
[6] *Russian Quantum Center, Skolkovo, Moscow 143025, Russia*

(Dated: March 3, 2020)

SUPPLEMENTARY NOTE 1: CIRCUIT DESIGN

The granular aluminum oxide nanowire oscillator can be described by an equivalent circuit diagram (Supplementary Figure 1) in terms of a series connection of capacitance, linear inductance and non-linear inductance. On chip, two pads ($60 \times 160\,\mu m^2$) constitute the capacitance. These are shunted by the nanowire contributing the non-linear inductance. Since the whole oscillator is made from a high kinetic inductance material, all circuit elements contribute additional inductance that acts linearly due to their higher critical currents.

For readout and manipulation, the non-linear oscillator is capacitively coupled to a classical harmonic resonator. This is realized in a meandered aluminum $\lambda/2$ geometry. At low temperatures ($T \ll 1\,K$) the excitation of the nanowire oscillator influences the harmonic resonator's frequency. This is used in a dispersive manipulation and readout scheme [1].

The circuit is connected to the measurement setup by two port transmission through a microwave feedline.

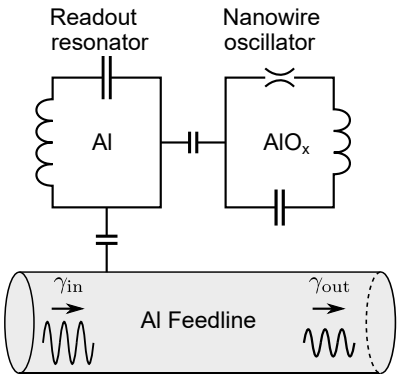

Supplementary Figure 1. Schematic circuit diagram of the experiment. The granular aluminum oxide nanowire oscillator can be described as nonlinear LC-oscillator with its inductance split between the nonlinear contribution of the nanowire and the linear part in the capacitive paddles. It is coupled to a harmonic aluminum readout resonator with a resonance frequency depending on the circuit's state [1]. The connection to the measurement setup is established by a two port microwave transmission line.

SUPPLEMENTARY NOTE 2: SPECTROSCOPY

To detect transitions in the nanowire circuits, a dispersive two-tone spectroscopy scheme is used. At one fixed frequency, the resonance dip of the readout resonator is monitored while a second drive tone is swept over a given frequency range. The coupling between the readout resonator and the sample circuit results in a shift of the readout resonance frequency when a transition is excited [1]. This shift leads to a change in the measured amplitude and phase. Supplementary Figure 2 depicts data of three sample circuits. The increased drive power required for direct spectroscopy of multi-photon transitions [2] to higher levels result in a broadening of the fundamental transition. Thus, individual lines of higher levels are not resolved.

SUPPLEMENTARY NOTE 3: NUMERICAL MODELING

In order to understand the interplay of the circuit anharmonicity and potential multi-photon effects due to the microwave driving of the circuit, we simulate the system using the following model. The undriven Hamiltonian of the system is given by

$$\mathcal{H}_0 = h(f_{01} + f_s\sqrt{\epsilon^2/(\epsilon^2+\Delta^2)})\hat{n} - hf_{an}(\hat{n}^2 - \hat{n}) \quad \text{(S.eq.1)}$$

with the bosonic number operator $\hat{n}$. This describes an oscillator with frequency f_{01} and anharmonicity f_{an}. A value of 1.3 MHz for f_{an} is found to agree with other measurements (Fig. 2b in main text). An additional asymmetry extending toward the off resonant regions in the measurement is accounted for by a slight shift f_s of the main transition in a region defined by a parameter for the width ϵ and reduced with the detuning Δ of the drive. This shift might be due to an AC stark effect [3]. In the

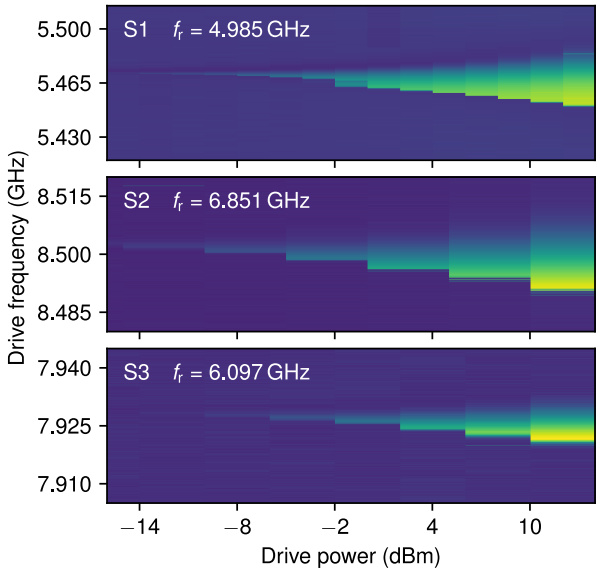

Supplementary Figure 2. Two-tone spectroscopy of the three samples. If a second microwave drive excites transitions in the sample circuit, the measured amplitude at a fixed frequency in the readout resonance shifts (encoded in the colormap). Due to the line broadening at higher drive power, higher transitions do not show as separate lines.

shown result (Fig. 3b in main text) f_s was set to -2 MHz and ϵ to 1 MHz, both adjusted to the off resonant region.

As we are specifically interested in replicating the observed Rabi oscillations, we also need to include the effects of decoherence. We do this by solving the Lindblad-GKS equation [4, 5],

$$\dot{\rho} = -\mathrm{i}/\hbar[\mathcal{H}, \rho] + \sum_{j=1}^{N} \Gamma_j [L_j \rho L_j^\dagger - 1/2\{L_j^\dagger L_j, \rho\}] \quad \text{(S.eq.2)}$$

numerically. In this case the total Hamiltonian is comprised of the undriven component and the drive term

$$\mathcal{H} = \mathcal{H}_0 + \mathcal{H}_{\mathrm{drive}} \quad \text{(S.eq.3)}$$

where for this circuit we assume that

$$\mathcal{H}_{\mathrm{drive}} = a + a^\dagger \quad \text{(S.eq.4)}$$

with the ladder operators defined in the basis of the undriven Hamiltonian such that $\hat{n} = a^\dagger a$. The drive amplitude was adapted to the off-resonant edges with a value of 0.0023.

For weak microwave driving we could move to a rotating frame to work with a time-independent Hamiltonian. However due to the small anharmonicity we will need to include the possibility of multi-photon transitions. This can be achieved using a Floquet theory [6] approach.

The decoherence channels of the Lindblad equation are encoded via the operators L_j and their corresponding rates Γ_j. The effects of energy dissipation are included via the operator

$$L_1 = a, \quad \text{(S.eq.5)}$$

allowing for a decay of one step down. Dephasing is included via

$$L_2 = a^\dagger a. \quad \text{(S.eq.6)}$$

To reduce the amount of dynamic parameters, the rates have been fixed to 4 µs energy lifetime and 1 µs dephasing time, in the order of results from time domain measurements.

To solve the Lindblad equation using Floquet theory, we express the system in an expanded space using the approach detailed in Ref. [7]. We then solve the resulting matrix exponential as a function of time, resumming the contributions due to the various Floquet components to obtain the population of the relevant states. From this we calculate the sum of the occupation probability of each state multiplied by a factor of $\sqrt{N}$ to obtain the measurement signal. The additional factor attributes for a reduced dispersive shift of the higher excitations. Convergence of the numerical solution is achieved by increasing both the number of photon manifolds in the Floquet expansion and the number of anharmonic levels in the circuit until the results do not change noticeably. For the calculation of Fig. 3b in the main text, this required 6 Floquet states and 5 circuit levels.

To account for the remaining differences between this model and measurement, several factors can be pointed out. Most importantly, the model Hamiltonian is of a phenomenological form, representing an oscillator with simple anharmonicity. The precise form, however, depends on the exact current phase relation in the system which at this point is not known. Especially at the region in which higher transitions are excited, two further simplifications play a role. It is assumed that both the decay rates and the coupling to the drive will differ between the levels. As there is no way of directly measuring the corresponding rates, we favored a simpler model with fewer free parameters.

* rotzinger@kit.edu

[1] Blais, A., Huang, R.-S., Wallraff, A., Girvin, S. M. & Schoelkopf, R. J. Cavity quantum electrodynamics for superconducting electrical circuits: An architecture for quantum computation. *Physical Review A* **69**, 062320 (2004).

[2] Braumüller, J. *et al.* Multiphoton dressing of an anharmonic superconducting many-level quantum circuit. *Physical Review B* **91**, 054523 (2015).

[3] Schneider, A. *et al.* Local sensing with the multilevel ac Stark effect. *Physical Review A* **97**, 062334 (2018).

[4] Lindblad, G. On the generators of quantum dynamical semigroups. *Communications in Mathematical Physics* **48**, 119–130 (1976).

[5] Gorini, V., Kossakowski, A. & Sudarshan, E. C. G. Completely positive dynamical semigroups of N-level systems. *Journal of Mathematical Physics* **17**, 821–825 (1976).

[6] Shirley, J. H. Solution of the Schrödinger equation with a Hamiltonian periodic in time. *Physical Review* **138**, B979–B987 (1965).

[7] Bain, A. D. & Dumont, R. S. Introduction to Floquet theory: The calculation of spinning sideband intensities in magic-angle spinning NMR. *Concepts in Magnetic Resonance* **13**, 159–170 (2001).